Electron Scattering and Muon Capture by C^{12} and O^{16} in a Continuum Model*

J. L. FRIAR†

Institute of Theoretical Physics, Department of Physics, Stanford University, Stanford, California 94305 and University of Washington, Seattle, Washington

(Received 14 April 1969; revised manuscript received 18 August 1969)

The giant resonance region of C^{12} and O^{16} is investigated using a continuum model, which is based on configuration mixing of negative-parity particle-hole states, with the particle in the continuum. Using this model $T=1$, $J^\pi=1^-$, and 2^- electron-scattering spectra are calculated as well as the 0^-, 1^-, and 2^- nuclear-excitation spectra (or equivalently the neutrino spectra) in μ capture. The $SU(4)$ relationship $M_P^2=M_V^2=M_A^2$ is tested and found to be satisfied in both nuclei to better than 10%. In addition, the relationship $(M_V^2)=(M_V^2)_{UD}\,|\,F_{el}(\nu_{res}^2)|^2$ is tested and found to hold to within 3%. Both of these results justify the previous work of Foldy and Walecka on calculations of total-muon-capture rates. The detailed behavior of the electron scattering spectra is examined as a function of momentum transfer with emphasis on the magnetic contribution to the 1^- transverse electric spectra and the giant magnetic quadrupole resonances. The momentum dependence of integrated form factors for certain regions of the excitation spectra is also investigated.

INTRODUCTION

THE purpose of this work is to examine the structure of C^{12} and O^{16}, both closed-shell nuclei, in the giant resonance region of the excitation spectrum. Electron scattering and muon capture are excellent tools for studying this structure because their interactions are relatively weak. Both interactions have sufficiently small coupling constants that it is unnecessary to treat the coupled problem of nuclear physics plus external interaction. One need only treat the electron's electromagnetic interaction or the muon's weak interaction in the Born approximation, which is another way of saying that these interactions do not mix nuclear states. Proton-nucleus scattering has just this disadvantage.

Electron scattering and photoabsorption are closely related processes. Both are electromagnetic, but photoabsorption is rather limited in the amount of information that can be derived from it. Real photons can only transfer equal amounts of energy and momentum, $q_\mu^2=0$. Electron scattering, on the other hand, allows independent variation of q (momentum transfer) and ω (energy loss) subject to the constraint $q_\mu^2>0$. Whereas photoabsorption produces a single energy spectrum, electron scattering can produce an energy spectrum for each momentum transfer.[1–7]

Muon capture contains much less information than electron scattering, because momentum transfer and energy loss are linearly related as they are in photoabsorption. There are, however, several different transition operators which contribute to muon capture, which increases the amount of information one can derive from the process.

Previous theoretical work on total muon-capture rates by Foldy and Walecka[8] has pointed out the dominant role of the $T=1$, $J^\pi=0^-$, 1^-, and 2^- states lying in the giant resonance region in the μ-capture process. Their work, based on the assumption of $SU(4)$ invariance, contains a number of predictions which have been tested in a number of models.[9–17] One of the purposes of this work is to examine the assumptions of Foldy and Walecka in a continuum nuclear shell model.

Electron scattering work has shown that there is interesting structure in the spectrum of the giant resonance region. The theoretical work of Lewis, deForest, and Walecka,[1–4] and the experimental work of Barber, Goldemberg, and vanPraet[5–7] indicate that there are strong magnetic contributions to the 1^- transverse electric form factors. We wish to calculate and examine the two-dimensional surfaces in momentum transfer

* Research sponsored in part by the Air Force Office of Aerospace Research, U.S. Air Force, under AFOSR Contract No. F44620-68-C-0075, and by the U.S. Atomic Energy Commission Contract No. AT(45-1)-1388.

† Present address: Department of Physics, University of Washington, Seattle, Wash.

[1] F. H. Lewis, Jr., and J. D. Walecka, Phys. Rev. **133**, B849 (1964).
[2] F. H. Lewis, Jr., Phys. Rev. **134**, B331 (1964); **138**, AB5(E) (1965).
[3] F. H. Lewis, Jr., J. D. Walecka, J. Goldemberg, and W. C. Barber, Phys. Rev. Letters **10**, 493 (1963).
[4] T. deForest, Jr., Phys. Rev. **139**, B1217 (1965).
[5] J. Goldemberg and W. C. Barber, Phys. Rev. **139**, B968 (1964).
[6] G. J. VanPraet and W. C. Barber, Nucl. Phys. **79**, 550 (1966).
[7] G. J. VanPraet, Nucl. Phys. **74**, 219 (1965).
[8] L. L. Foldy and J. D. Walecka, Nuovo Cimento **34**, 1026 (1964).
[9] V. V. Balashov, G. Ya. Korenman, V. L. Korotkikh, and V. N. Fetishov, Nucl. Phys. **B1**, 158 (1967).
[10] V. V. Balashov, V. B. Beliaev, R. A. Eramjian, and N. M. Kabachnik, Phys. Letters **9**, 168 (1964).
[11] V. V. Balashov and R. A. Eramzhyan, At. Energy Rev. **5**, 3 (1967).
[12] M. Rho, Phys. Letters **16**, 161 (1965); **18**, 671 (1967); **19**, 248 (1967); Phys. Rev. **161**, 955 (1967).
[13] H. Uberall, Nuovo Cimento **38**, 669 (1965); Phys. Rev. **139**, 1239 (1965).
[14] R. Raphael, H. Uberall, and C. Werntz, Phys. Letters **24B**, 15 (1967).
[15] B. R. Barrett, Phys. Rev. **159**, 816 (1967).
[16] G. E. Walker, Phys. Rev. **151**, 745 (1966); **157**, 854 (1967).
[17] L. L. Foldy and R. H. Klein, Phys. Letters **24B**, 540 (1967).

and energy loss as seen in electron scattering. Early attempts to understand electromagnetic form factors of C^{12} and O^{16} were made by Lewis and Walecka.[1-3] Their work was a reformulation of previous models in terms of the Tamm-Dancoff approximation. The approximation allows a consistent reduction of the nuclear Hamiltonian into a single-particle configuration Hamiltonian and a residual particle-hole Hamiltonian. This was accomplished by writing the excited state of the nucleus as a linear combination of shell-model particle-hole states and keeping only those terms in the Hamiltonian which contribute to particle-hole matrix elements. This formalism was then used by de-Forest[4] to study quadrupole excitations (2^-) in C^{12} and O^{16}, as well as partial muon-capture rates into 0^-, 1^-, and 2^- states.

These calculations, however, do not emphasize an important aspect of the giant resonance region. Many of the "states" in this region lie above single-particle emission thresholds.[18-36] Thus, rather than being bound, these states are resonances. A model originally introduced by Weiss and Villars[24] has been quite versatile in handling both electron scattering and muon capture. The important aspects are the following. The excited states are assumed to consist only of linear combinations of holes and particles in the continuum or high-lying bound states [Tamm-Dancoff approximation]. The Hamiltonian is reduced to a single-particle Hartree-Fock potential and a particle-hole "residual" interaction. The single-particle potential is chosen to be a square well and is adjusted so that the states of neighboring nuclei correspond to experimental energies. The range of the potential is fixed by elastic electron scattering as calculated in the model and compared with experiment. Even though the square-well potential may be an unrealistic Hartree-Fock potential, it gives a ground-state charge density which produces a charge form factor that allows a good fit for $q \leq 200$ MeV/c. A phenomenological residual potential is introduced which reduces the excited-state coupled integral equations to a set of matrix equations which are then solved numerically. Transition matrix elements can then be computed.

NUCLEAR PHYSICS

There are really two separate problems which must be solved in the giant resonance region. First of all, there are bound states which lie below the particle-emission thresholds. This causes no great difficulty in a model such as the harmonic-oscillator shell model (HOSM), because it is only necessary to diagonalize a secular matrix to obtain eigenvalues and then calculate eigenvectors. The bound-state problem is somewhat more complicated in a model with a finite potential, but in our model the solution is obtained in a similar manner. Unbound states are quite different, however, and must be handled differently.

We separate the nuclear many-body Hamiltonian into three parts. One part consists of the (diagonal) Hartree-Fock Hamiltonian, the second is the particle-hole interaction potential, while the third contributes no matrix element between particle-hole states and is neglected. We can therefore write

$$\hat{H}=\hat{H}_0+\hat{V}, \tag{1}$$

and, since the excited-state wave function must have incoming wave boundary conditions, we have

$$\psi_f^{(-)}(E)=\phi_f^{(-)}(E)+[1/(E-\hat{H}_0-i\epsilon)]\hat{V}\psi_f^{(-)}(E). \tag{2}$$

Since we restrict ourselves to one-particle–one-hole excited states and uncorrelated ground states, $\phi_f^{(-)}(E)$ is a shell-model state. Projecting out states of total angular momentum J and total isotopic spin T, we can write

$$\psi_{[\alpha]k\alpha}^{(-)}=\phi_{\alpha,k\alpha}^{(-)}+\sum_{\beta,k_\beta}[\phi_{\beta,k\beta}/(E-E_\beta-i\epsilon)] \times\langle\phi_{\beta,k\beta}\mid\hat{V}\mid\psi_{[\alpha],k\alpha}^{(-)}\rangle, \tag{3}$$

where the explicit dependence on the diagonal quantum numbers ($JMTM_T$) has been ignored, and the sum is over both bound and continuum states. The

---

[18] M. Bauer, University of Maryland Technical Report No. 260, 1962 (unpublished).
[19] R. H. Lemmer, Phys. Letters **4**, 205 (1963); R. H. Lemmer and C. M. Shakin, Ann. Phys. (N.Y.) **27**, 13 (1964).
[20] J. Eichler, Nucl. Phys. **56**, 577 (1964).
[21] H. J. Mikeska, Z. Physik **177**, 441 (1964).
[22] E. Boeker and C. C. Jonker, Phys. Letters **6**, 80 (1963).
[23] C. Bloch and V. Gillet, Phys. Letters **16**, 62 (1965); V. Gillet and C. Block, *ibid.* **18**, 58 (1965).
[24] F. Villars and M. S. Weiss, Phys. Letters **11**, 318 (1964); M. S. Weiss, *ibid.* **19**, 393 (1965); J. L. Friar, Nucl. Phys. **84**, 150 (1966).
[25] W. M. MacDonald, Nucl. Phys. **54**, 393 (1964); **56**, 636 (1964); **56**, 647 (1964); Phys. Rev. **137**, B1438 (1965); L. Garside and W. M. MacDonald, *ibid.* **138**, B582 (1965).
[26] W. P. Beres, Phys. Rev. Letters **17**, 1180 (1966); W. P. Beres and W. M. MacDonald, Nucl. Phys. **A91**, 529 (1967).
[27] M. Danos and W. Greiner, Phys. Rev. **138**, B93 (1965); **146**, 708 (1966).
[28] M. Bauer and F. Prats, Nucl. Phys. **89**, 230 (1966); A. Agodi, F. Catara, M. DiToro, and O. Stazi, Nuovo Cimento **B48**, 237 (1967).
[29] V. V. Balashov, P. Doleshal, G. Ya. Korenman, V. L. Korotkikh, and V. N. Fetsihov, Yadern. Fiz. **2**, 643 (1965) [English transl.: Soviet J. Nucl. Phys. **2**, 461 (1966)]; V. V. Balashov and N. M. Kabachnik, Phys. Letters **25B**, 316 (1967); N. M. Kabachnik, V. L. Korotkikh, and G. Yu. Unger, Nucl. Phys. **A103**, 450 (1967); Yadern. Fiz. **6**, 973 (1967) [English transl.: Soviet J. Nucl. Phys. **6**, 708 (1968)].
[30] V. Gillet, M. A. Melkanoff, and J. Raynal, Nucl. Phys. **A97**, 631 (1967); J. Raynal, M. A. Melkanoff, and T. Sawada, *ibid.* **A101**, 369 (1967).
[31] H. A. Wahsweiler, W. Greiner, and M. Danos, Phys. Letters **23**, 257 (1966); Phys. Rev. Letters **17**, 395 (1966); Phys. Rev. **170**, 893 (1968); P. Antony-Spies, W. Donner, H. G. Wahsweiler, and W. Greiner, Phys. Letters **26B**, 268 (1968).
[32] B. Buck and A. D. Hill, Nucl. Phys. **A95**, 271 (1967); M. Marangoni and A. M. Sarius, Phys. Letters **24B**, 218 (1967).
[33] S. Fujii, Phys. Letters **24B**, 7 (1967).
[34] P. J. A. Buttle, Phys. Rev. **160**, 719 (1967).
[35] W. Tobocman and M. A. Nagarajan, Phys. Rev. **163**, 1011 (1967); W. Tobocman, *ibid.* **166**, 1036 (1968).
[36] H. A. Weidenmuller, Nucl. Phys. **75**, 189 (1966); W. Glockle, J. Hufner, and H. A. Weidenmuller, *ibid.* **A90**, 481 (1967); C. Mahaux and H. A. Weidenmuller, Phys. Rev. **170**, 847 (1968).

channel label α refers to $[ljJ_h\alpha_h]$, where l and j are the particle orbital and total angular momenta, J_h is the hole angular momentum, and α_h is the rest of the quantum numbers needed to specify the hole state.

The solution to this set of integral equations is facilitated by using the surface-δ interaction

$$V(\mathbf{x}_1, \mathbf{x}_2) = V_0 r_0^2 \delta(\,|\,\mathbf{x}_1\,|\,-r_0)\,\delta(\,|\,\mathbf{x}_2\,|\,-r_0)\,\delta(\hat{x}_1-\hat{x}_2)\,(1-\lambda+\lambda\boldsymbol{\delta}_1\cdot\boldsymbol{\delta}_2), \quad (4)$$

where r_0 is the well radius, $\lambda=0.135$, and V_0 is the over-all potential strength. We write the excited state as a linear combination of shell-model particle-hole states

$$\psi_{[\alpha]}{}^{(-)}(E) = \sum_{\beta=\beta_p\beta_h} [\int k'^2 dk' C_{\beta k'}{}^{\alpha}(E)\,\phi_{\beta k'}{}^{(-)} + B_\beta{}^{\alpha}(E)\,\phi_\beta{}^{b}], \quad (5)$$

where superscripts refer to the continuum and bound contributions, while β_p, β_h refer to particle and hole single-particle quantum numbers. We can solve for the coefficients in the manner previously reported.[24] Defining

$$R_\beta{}^{\alpha(-)}(k, r) = \int k'^2 C_{\beta k'}{}^{\alpha}(E)\,R_{\beta_p}{}^{(-)0}(k', r)\,dk' + B_\beta{}^{\alpha}(E)\,R_{\beta_p}{}^{b0}(r), \quad (6)$$

we can write

$$R_\beta{}^{\alpha(-)}(k, r) = R_\beta{}^{(-)0}(k, r) + V_0 r_0^3 [G_{\beta,E}{}^{(-)}(r, r_0) + G_{\beta,E}{}^{b}(r, r_0)] \times \sum_\gamma f_{\beta\gamma}{}^{JT} R_\gamma{}^{\alpha(-)}(k, r_0), \quad (7)$$

where the G's are single-particle Green's functions, and $f_{\beta\gamma}{}^{JT}$ is the angular part of the potential matrix element in Eq. (3).

For computational purposes, it is convenient to "solve" for the Green's function in terms of radial solutions of another single-particle potential. Consider the potential

$$u(r) = V_{SQ}(r) + V r_0 \delta(r-r_0). \quad (8)$$

The incoming wave solutions of this equation are the radial wave functions

$$R_\beta{}^{(-)}(k, r).$$

We can write

$$G_{\beta,E}{}^{(-)} + \sum_{N_\beta} G_{\beta,E}{}^{b}(r, r_0) = (1/V r_0^3) \times \{[R_\beta{}^{(-)}(k, r) - R_\beta{}^{(-)0}(k, r)]/R_\beta{}^{(-)}(k, r_0)\}, \quad (9)$$

where the sum is over all configuration bound states with quantum numbers β. In light nuclei such as C^{12} and O^{16}, only the $s_{1/2}$ single-particle channel has two bound states. One of these is the bound (and filled) $1s_{1/2}$ shell. The Pauli exclusion principle forbids transitions into this shell, so the Green's function in Eq. (7) lacks the term. Defining

$$f_{\beta\gamma}{}'^{JT} = f_{\beta\gamma}{}^{JT}/f_{\beta\beta}{}^{JT}$$

and

$$V_\beta' = V_0 f_{\beta\beta}{}^{JT},$$

we get

$$R_\beta{}^{\alpha(-)}(k, r) = R_\alpha{}^{(-)0}(k, r)\,\delta_{\alpha\beta} + \frac{[R_\beta{}^{(-)}(k, r) - R_\beta{}^{(-)0}(k, r) - V_\beta' r_0^3 G_\beta{}^{b}(r, r_0)]}{R_\beta{}^{(-)}(k, r_0)} \times \sum_\gamma f_{\beta\gamma}{}^{JT} R_\gamma{}^{\alpha(-)}(k, r_0). \quad (10)$$

Everything in the above equation is known analytically. Furthermore, if the diagonal matrix elements of $f_{\beta\gamma}{}^{JT}$ are dominant, we can approximate

$$R_\beta{}^{\alpha(-)}(k, r) \approx R_\beta{}^{(-)}(k, r)\,\delta_{\alpha\beta}.$$

The bound-state equations can be similarly solved. The single-particle radial equation for a bound state in this model is

$$R_\beta{}^{b}(E, r) = V' r_0^3 [G_{\beta,E}{}^{(-)}(r, r_0) + \sum_{N_\beta} G_{\beta,E}{}^{b}(r, r_0)] \times R_\beta{}^{b}(E, r_0), \quad (11)$$

with the obvious restriction that V_β' and E are not independent and cannot be varied independently. Setting $r=r_0$ in the above equation yields the eigenvalue equation. For purposes of finding a solution to the bound-state problem, we want the Green's function as a function of energy so we write

$$V' = V_\beta'(E),$$

where $V_\beta'(E)$ is the potential necessary to produce an eigenvalue at an energy E. We therefore write

$$R_\beta{}^{ab}(E, r) = [V_0/V_\beta'(E)] \times \left(\frac{R_\beta{}^{b}(E, r)}{R_\beta{}^{b}(E, r_0)} - V_\beta'(E)\,r_0^3 G_{\beta,E}{}^{b}(r, r_0)\right) \times \sum_\gamma f_{\beta\gamma}{}^{JT} R_\gamma{}^{ab}(E, r_0). \quad (12)$$

As before, we subtract off any filled bound states because of the Pauli principle. Defining

$$V_{\alpha\beta} = V_0 f_{\alpha\beta}{}^{JT}[1 - V_\beta'(E)\,r_0^3 G_{\beta,E}{}^{b}(r_0, r_0)], \quad (13)$$

we get

$$\sum_\gamma [\delta_{\beta\gamma} V_\beta'(E) - V_{\beta\gamma}] R_\gamma{}^{ab}(E, r_0) = 0, \quad (14)$$

which is almost identical to what one gets in the usual bound-state models. Neglecting the small correction term, we have

$$R_\beta{}^{ab}(E_\alpha, r) = D_\beta{}^{\alpha}(E_\alpha)\,R_\beta{}^{b}(E_\alpha, r), \quad (15)$$

with

$$\sum_\gamma D_\gamma{}^{\alpha} D_\gamma{}^{\alpha *} = 1. \quad (16)$$

In nuclei such as C^{12} and O^{16}, there are several thresholds for particle emission. Channels which are below threshold have equations of motion which are the same as the bound states, although configuration

mixing couples them to continuum states in those channels above threshold. Therefore, we need only combine Eqs. (10) and (12) for channels above and below threshold to complete the problem. A knowledge of the functions R_β^α constitutes a solution to the problem, since we can write the transition matrix elements as

$$\langle\psi_{[\alpha]}\,||\,T\,||\,0\rangle=\sum_{\beta_p\beta_h}(\int k'^2dk'C_{\beta k'}{}^{\alpha}\langle\phi_{\beta k'}{}^{(-)}\,||\,T\,||\,0\rangle + B_\beta{}^\alpha\langle\phi_\beta{}^b\,||\,T\,||\,0\rangle). \quad (17)$$

The configuration state matrix elements can be put in the form $\langle\phi_\beta\,||\,T\,||\,0\rangle=\langle\beta_p\,|\,t_\beta\,|\,\beta_h\rangle$, where the latter matrix element is purely radial. Finally, we get

$$\langle\psi_{[\alpha]}\,||\,T\,||\,0\rangle=\sum_{\beta_p\beta_h}\langle R_\beta{}^\alpha\,|\,t_\beta\,|\,{}_{\beta_h}\rangle. \quad (18)$$

ELECTRON SCATTERING

The cross section for electron scattering can be expressed in terms of three form factors which contain all the nuclear physics.[37] These form factors (for exciting a closed-shell ground state into a $T=1$ excited state) are

$$F_J{}^{\rm el}(q,\omega)=\sum_\beta(k_\beta M)\,|\,\langle\beta J\,||\,\hat T_J{}^{\rm el}(q)\,||\,0\rangle\,|^2,$$

$$F_J{}^{\rm mag}(q,\omega)=\sum_\beta(k_\beta M)\,|\,\langle\beta J\,||\,\hat T_J{}^{\rm mag}(q)\,||\,0\rangle\,|^2, \quad (19)$$

$$F_J{}^{\rm Coul}(q,\omega)=\sum_\beta(k_\beta M)\,|\,\langle\beta J\,||\,\hat M_J(q)\,||\,0\rangle\,|^2,$$

where

$$\hat M_{JM}(q)=\int d\mathbf{x}\rho_N(\mathbf{x})j_J(qx)\mathfrak{Y}_{JM}(\hat x), \quad (20a)$$

$$\hat T_{JM}{}^{\rm el}(q)=(1/q)\int d\mathbf{x}[\,\mathbf{j}_N(\mathbf{x})\cdot\nabla\times j_J(qx)\mathfrak{Y}_{JJ1}{}^M(\hat x) + q^2j(qx)\mathfrak{Y}_{JJ1}{}^M(\hat x)\cdot\boldsymbol{\mu}_N(\mathbf{x})\,], \quad (20b)$$

$$\hat T_{JM}{}^{\rm mag}(q)=\int d\mathbf{x}[\boldsymbol{\mu}_N(\mathbf{x})\cdot\nabla\times j_J(qx)\mathfrak{Y}_{JJ1}{}^M(\hat x) + j_J(qx)\mathbf{j}_N(\mathbf{x})\cdot\mathfrak{Y}_{JJ1}{}^M(\hat x)\,] \quad (20c)$$

are the Coulomb, electric, and magnetic multipole operators, respectively. The operators $\rho_N(\mathbf{x})$, $\mathbf{j}_N(\mathbf{x})$, and $\boldsymbol{\mu}_N(\mathbf{x})$ are the nuclear charge, current, and magnetization densities, respectively, while $j_J(x)$ and $\mathfrak{Y}_{JJ1}{}^M(\hat x)$ are the usual spherical Bessel functions and vector spherical harmonics.[38] In the case of excitation to a bound state, the factor $(k_\beta M)$ is missing and only one term in the sum contributes at that energy.

We are primarily interested in the transverse matrix elements in electron scattering because their structure contains information about magnetic effects in nuclear excitation. In addition, abnormal parity states 1^+, 2^-, 3^+ can be excited by the transverse operators but not by the Coulomb interaction. Even though only the transverse matrix elements contribute to photoabsorption the kinematics restrict us to $q=\omega$; in electron scattering we have $q^2-\omega^2>0$.

There is a different way of analyzing the electric form factor, using current conservation. It can be shown[8] that a number of single-particle operators of the form

$$\hat O^1=\sum_{i=1}^A t_3(i)f(i) \quad (21)$$

and

$$\hat O_\lambda{}^2=\sum_{i=1}^A t_3(i)\sigma_\lambda(i)f(i)$$

"generate" the giant resonances. If we examine Eqs. (20a) and (20b) for $J=1$, we see that one of our operators is not of the above form.

If we keep only isovector terms in the operators and write them in first quantization form for small momentum transfers, we see that

$$\hat M_{1\lambda}=\sum_{i=1}^A t_3(i)x_\lambda(i)$$

and that the magnetic term in $\hat T_{1M}{}^{\rm el}$ is of the form

$$\hat T_{1\lambda}{}^{\rm el}\,|_{\rm mag}\sim\sum_{i=1}^A t_3(i)[\boldsymbol{\sigma}(i)\otimes\mathbf{x}(i)\,]_{1\lambda}.$$

However, the current dominates the total operator $T_{1M}{}^{\rm el}$ at small momentum transfers, and this is of the form

$$\hat T_{1\lambda}{}^{\rm el}\,|_{\rm current}\sim\sum_{i=1}^A t_3(i)\nabla_\lambda(i)\,|_{\rm sym.}$$

This is not one of the operators $\hat O$. Because of this, there is no way to use $SU(4)$ invariance[8] to analyze the low-momentum-transfer transitions induced by this operator. We can, however, reduce the dependence of the matrix element on the current (and eliminate it altogether at very small momentum transfers).

To accomplish this we write

$$\int d\mathbf{x}\,\mathbf{j}_N(\mathbf{x})\cdot\nabla\times j_J(qx)\mathfrak{Y}_{JJ1}{}^M(\hat x) \equiv\int d\mathbf{x}j_J(qx)\mathfrak{Y}_{JJ1}{}^M(\hat x)\cdot\nabla\times\mathbf{j}_N(\mathbf{x}). \quad (22)$$

We can use an identity involving the vector spherical harmonics to get

$$\int d\mathbf{x}\mathbf{j}_N(\mathbf{x})\cdot\nabla\times j_J(qx)\mathfrak{Y}_{JJ1}{}^M(\hat x) =\{-i/[J(J+1)]^{1/2}\}\int d\mathbf{x}\mathfrak{Y}_{JM}(\hat x) \times\{\nabla\cdot\mathbf{j}_N(\mathbf{x})\,(\partial/\partial x)\,(xj_J(qx)\,)-q^2\mathbf{x}\cdot\mathbf{j}_N(\mathbf{x})j_J(qx)\}. \quad (23)$$

Furthermore, we can use the continuity equation

$$\nabla\cdot\mathbf{j}_N(\mathbf{x})=-i[\hat H,\rho_N(\mathbf{x})\,]. \quad (24)$$

[37] T. deForest, Jr., and J. D. Walecka, Advan. Phys. **15**, 1 (1966).

[38] A. R. Edmonds, *Angular Momentum in Quantum Mechanics* (Princeton University Press, Princeton, N.J., 1957).

Inserting the above equation into Eq. (23) we get

$$\int d\mathbf{x}\mathbf{j}_N(\mathbf{x})\cdot\nabla\times j_J(qx)\mathcal{Y}_{JJ1}{}^M(\hat{x})$$
$$\{-i/[J(J+1)]^{1/2}\}\int d\mathbf{x}\mathcal{Y}_{JM}(\hat{x})$$
$$\times\{\omega_{fi}\rho_N(\mathbf{x})(\partial/\partial x)(xj_J(qx))-iq^2\mathbf{x}\cdot\mathbf{j}_N(\mathbf{x})j_J(qx)\}. \quad (25)$$

This recasting of the form of $\hat{T}_{JM}{}^{\mathrm{el}}$, which is well known as Siegert's theorem, has the desired form now. For small momentum transfers, we get

$$\hat{T}_{1\lambda}{}^{\mathrm{el}}|_{\mathrm{charge}}\sim\sum_{i=1}^{A}t_3(i)x_\lambda(i), \quad (26)$$

which is one of the "generators" of $SU(4)$. Furthermore, we do not expect the term proportional to $\mathbf{j}_N(\mathbf{x})$ to have a great effect. It is only significant at large momentum transfers, and that region is dominated by the magnetic term because of the large isovector magnetic moment in $T=1$ states. We define a new quantity $\hat{T}'_{JM}{}^{\mathrm{el}}$ corresponding to the transverse electric operator's new form

$$\hat{T}'_{JM}{}^{\mathrm{el}}=(1/q)\int d\mathbf{x}\{(-\mathcal{Y}_{JM}(\hat{x})/[J(J+1)]^{1/2})$$
$$\times[\omega_{fi}\rho_N(\mathbf{x})(\partial/\partial x)(xj_J(qx))-iq^2j_J(qx)\mathbf{x}\cdot\mathbf{j}_N(\mathbf{x})]$$
$$+q^2j_J(qx)\mathcal{Y}_{JJ1}{}^M(\hat{x})\cdot\boldsymbol{\mu}_N(\mathbf{x})\}. \quad (27)$$

Although we might suppose that $T'_{JM}{}^{\mathrm{el}}$ would give the same result as $\hat{T}_{JM}{}^{\mathrm{el}}$, we shall see that this is not true. The flaw lies in the use of the current continuity equation. This operator identity does not hold in this model for transition currents (although it does for regular currents). We can see this as follows. Construct the divergence of the single-particle current operator in second quantization:

$$\nabla\cdot\mathbf{j}_N(\mathbf{x})=(1/2im)\{\phi^\dagger(\mathbf{x})\nabla^2\phi(\mathbf{x})-\nabla^2\phi^\dagger(\mathbf{x})\phi(\mathbf{x})\}. \quad (28)$$

We also can write

$$(1/i)[\hat{H},\rho(\mathbf{x})]=(1/i)\{[\hat{H}_0,\rho(\mathbf{x})]+[\hat{V},\rho(\mathbf{x})]\}, \quad (29)$$

where $\hat{H}_0$ and $\hat{V}$ are the single-particle and two-body parts of the Hamiltonian. If the two-body operator contains no derivative terms, it commutes with $\rho(\mathbf{x})$. Separating the kinetic and potential parts of $\hat{H}_0$, we get

$$\nabla\cdot\mathbf{j}_N(\mathbf{x})+i[\hat{H},\rho(\mathbf{x})]=i\{\phi^\dagger(\mathbf{x})u(\mathbf{x})\phi(\mathbf{x})$$
$$-[u(\mathbf{x})\phi^\dagger(\mathbf{x})]\phi(\mathbf{x})\}. \quad (30)$$

If $u(\mathbf{x})$, the single-particle potential, contains derivative terms, spin-orbit terms, or depends on the angular momentum eigenvalues of the states (l, j), the right-hand side has nonzero transition matrix elements. Diagonal matrix elements are obviously zero.

This problem is peculiar to Tamm-Dancoff approximation calculations, and arises in all such calculations. On the one hand, we demand that configuration energies be taken from neighboring nuclei; it is necessary to do this in order to produce realistic spectra. On the other hand, we lose current conservation, which we will see does not affect the position of our states, but does affect transition strengths. We have already used current conservation in the derivation of the electron scattering cross-section formula. We have seen that this equation contains three form factors which are independent of one another except at $q=0$. In this limiting case, the Coulomb form factor is related to the transverse electric form factor by the continuity equation. Because the continuity equation is not valid here for inelastic transitions, these form factors are not properly normalized to one another at $q=0$. Lewis and Walecka[1] showed that this difference was approximately a factor of $(\omega/\omega_0)^2$, where ω is the energy of the state in question and ω_0 is the harmonic-oscillator energy spacing. This amounts to a factor of 2 or less for most states. Although our two ways of evaluating the transverse electric form factor are not equivalent for $q=0$, we hope that normalized *form factors* for individual states in the absence of the magnetic part of $\hat{T}_{\mathrm{el}}$ will have the same dependence on momentum transfer in the two cases and we will show this to be approximately true in some simple examples.

MUON CAPTURE

The other process which is to be examined is μ capture, $\mu^-+N(A,Z)\rightarrow\nu+N(A,Z-1)$. Neglecting small nuclear recoil terms, the transition rate can be expressed in terms of three form factors

$$dM_{V,P}{}^2/d\omega=2\pi\sum_{\beta J}(\nu/M_\mu)^2(k_\beta M)\,|\,\langle\beta JT=1\;M_T=0\,||\,\hat{O}_{V,P}(\nu)\,||\,0\rangle\,|^2, \quad (31)$$

$$dM_A{}^2/d\omega=2\pi\sum_{\beta J}(\nu/M_\mu)^2(k_\beta M)\sum_L[(2L+1)/3]\,|\,\langle\beta JT=1\;M_T=0\,||\,\hat{O}_A{}^L(\nu)\,||\,0\rangle\,|^2, \quad (32)$$

where the single-particle operators are

$$O_V=\tau_3 j_J(\nu x)\mathcal{Y}_{JM}(\hat{x}),$$
$$O_P=\tau_3\{[J/(2J+1)]^{1/2}j_{J-1}(\nu x)(\mathcal{Y}_{J-1}\otimes\sigma)_{JM}+[(J+1)/(2J+1)]^{1/2}j_{J+1}(\nu x)(\mathcal{Y}_{J+1}\otimes\sigma)_{JM}\}, \quad (33)$$
$$O_A{}^L=\tau_3 j_L(\nu x)(\mathcal{Y}_L\otimes\sigma)_{JM}.$$

Furthermore, we can simplify these expressions by keeping only the dipole terms [$L=1$ in $\mathcal{Y}_{LM} j_L(\nu x)$]. The octupole contribution is considerably smaller and contributes to 2^-, 3^-, and 4^- states. We are only interested in the 0^-, 1^-, and 2^- contributions because they are by far the largest. Furthermore, the octupole contribution will largely cancel out of the total 2^- contribution if $SU(4)$ invariance holds. For these reasons we ignore the octupole terms.

We wish to investigate two things in μ capture using our model. The first is to test the validity of the relationship derived from $SU(4)$ invariance

$$M_V^2 = M_A^2 = M_P^2, \tag{34}$$

where

$$M^2 = \int_{\omega_2}^{\omega_1} \frac{dM^2}{d\omega}\, d\omega \tag{35}$$

and ω_1 and ω_2 are appropriate upper and lower limits to catch all the contribution of $dM^2/d\omega$ to the integral. The second relation to be tested is

$$M_V^2\,|_D = M_V^2\,|_{UD}\,|\,F_0(\nu_{\rm res}^2)\,|^2, \tag{36}$$

where $F_0(\nu_{\rm res}^2)$ is the elastic form factor evaluated at $\nu_{\rm res}$, the momentum transfer corresponding to the giant resonance energy, and $(M^2)_D$ is obtained by making the replacement

$$j_1(\nu x) \rightarrow \tfrac{1}{3}\nu x$$

in all radial matrix elements.

CALCULATIONS AND DISCUSSION OF RESULTS

In our discussion we will treat the two nuclei C^{12} and O^{16} separately. We take the case of C^{12} first.

The single-particle configuration energies were obtained from the energy level data of C^{11}, C^{12}, and C^{13}. From these nuclei, the particle-hole configuration energies listed below were obtained:

$$E^0((2s_{1/2})(1p_{3/2})^{-1}) = 16.86 \text{ MeV},$$

$$E^0((1d_{5/2})(1p_{3/2})^{-1}) = 17.62 \text{ MeV},$$

$$E^0((d_{3/2})(1p_{3/2})^{-1}) = 22.11 \text{ MeV}.$$

In addition to these there is another possible particle-hole state $((1p_{1/2})(1s_{1/2})^{-1})$ which is included in many C^{12} calculations. It was not included because the state must lie above 30 MeV and this is not in the range of interest here. The state has not been seen in electron scattering results.

With the above energies, the depths of the single-particle potentials and the square-well radius r_0 could be calculated by using the known value of the rms radius[39]

$$R_{\rm rms} = 2.42 \pm 0.04 \text{ fm}.$$

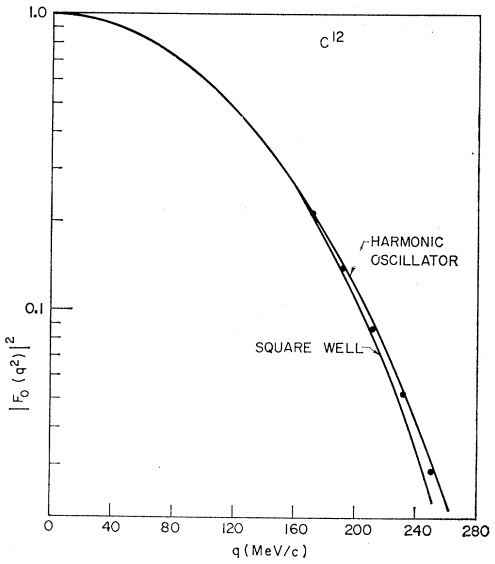

FIG. 1. C^{12} elastic scattering form factor versus momentum transfer. The data are from Ref. 42.

In the standard fashion, we write

$$r_0 = r_0' A^{1/3}$$

and get as a result (for $A=12$)

$$r_0' = 1.40 \text{ fm}.$$

The ground-state elastic scattering form factor $|\,F_0(q^2)\,|^2$ was then calculated. The result is plotted in Fig. 1. We have also plotted the result of the harmonic-oscillator shell model as a comparison (the length parameter b in this model was fitted to the rms radius also). We see that both models give fits which are indistinguishable for momentum transfers less than 140 MeV/c. The results diverge at this point although the experiments seem to lie midway between the two lines out to 210 MeV/c. From this point, the square-well model appears to be consistently low. We note, however, that good agreement is achieved over $1\frac{1}{2}$ decades and the behavior of the form factor in the vicinity of the diffraction minimum ($\sim$350 MeV/c) should be very sensitive to the nuclear model. While we do not claim that we have given a good fit to the elastic form factor at all momentum transfers, we do get good agreement below 200 MeV/c, which is the upper limit of interest in this work. This means that our nuclear charge density fits quite well to a depth of about 1 fm. Although it should not be very important for $q<200$ MeV/c, the effect of c.m. motion has not been taken into account. This would be very difficult in our model, although it is trivial in the harmonic-oscillator model.[40] c.m. motion can be accounted for in this case by multiplying the shell-model matrix elements

[39] R. Engfer and D. Turck, Z. Physik **205**, 90 (1967).

[40] L. J. Tassie and F. C. Barker, Phys. Rev. **111**, 940 (1958).

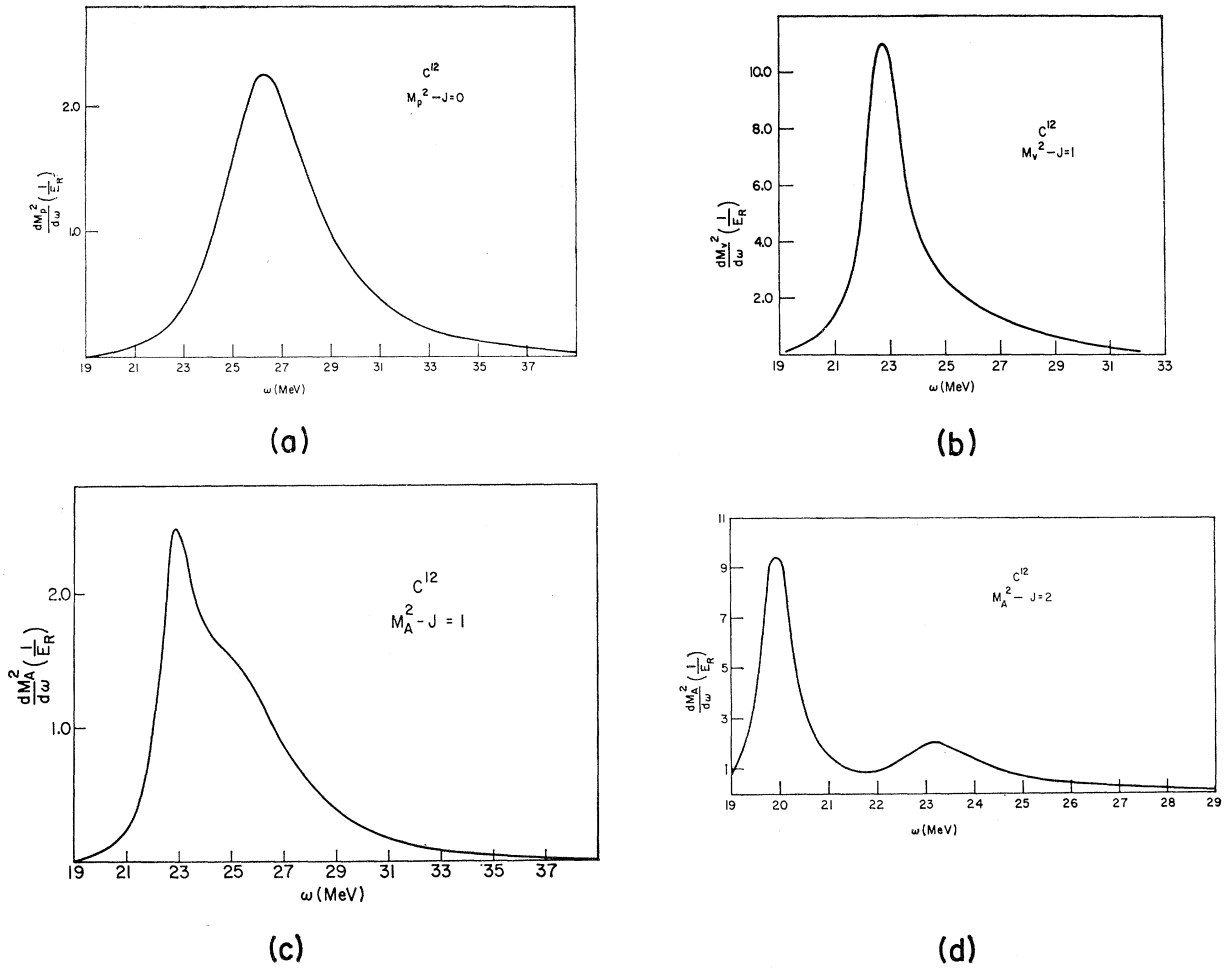

FIG. 2. C^{12} μ-capture spectrum. (a) $dM_P^2/d\omega$ for $J=0$. (b) $dM_V^2/d\omega$ for $J=1$. (c) $dM_A^2/d\omega$ for $J=1$. (d) $dM_A^2/d\omega$ for $J=2$. E_R is $(\hbar c/r_0)$ $(=61.56$ MeV).

by $\exp(q^2b^2/4A)$, where b is the oscillator parameter and A is the number of nucleons. This is small ($<10\%$) for $q<200$ MeV/c. With the single-particle potentials and potential-well radius determined, we calculated the coefficients $f_{\alpha\beta}{}^{JT}$ and then the photoabsorption cross section for various values of V_0, the over-all strength of the particle-particle potential. A value of V_0 was chosen so that the largest state in the spectrum, the giant resonance, has the experimentally observed energy of 22.8 MeV. We get $V_0=-32.9$ MeV. This completed the determination of the parameters of C^{12}.

Detailed spectra for 1^- and 2^- states may be obtained from electron scattering form factors, and for the 0^- (as well as the 1^- and 2^-) state from μ capture. Although we will discuss these spectra later in detail, it is desirable to list the resonant states we get in Table I. We have included the two 1^- and 2^- bound states for completeness. We can get some idea of the widths of the various resonances by examining the μ-capture spectra. Examining the $M_V^2(J=1)$ contribution [Fig. 2(b)], we see that the full width at half-maximum is 1.75 MeV for the 22.8-MeV giant state. The $M_A^2(J=1)$ contribution [Fig. 2(c)] allows us to estimate the width of the 25.6-MeV state to be 4 MeV. Figure 2(a) shows that the width of the $J=0$ state is about 4 MeV also. The two $J=2$ states can be seen in Fig. 2(d). They have widths of about 0.8 MeV (20.0-MeV state) and 2.5 MeV (23.2-MeV state). These widths are necessarily estimates since the states blend into each other and cannot easily be separated.

TABLE I. Energies of bound states and resonances in C^{12}. Energy in MeV.

$J=0$	$J=1$	$J=2$
26.2	17.75	17.19
	22.8	20.0
	25.6	23.2

TABLE II. Configuration mixing parameters for the bound states in HOSM and continuum model for C^{12}.

		$((s_{1/2})(p_{3/2})^{-1})$	$((d_{5/2})(p_{3/2})^{-1})$	$((d_{3/2})(p_{3/2})^{-1})$
	17.75 MeV			
$J=1$	Continuum	0.921	0.316	−0.229
	Harmonic oscillator	0.978	−0.164	0.127
	17.19 MeV			
$J=2$	Continuum	0.824	0.566	0.044
	Harmonic oscillator	0.937	−0.349	−0.025

The resonance states can be classified according to the configuration states which contribute to them most strongly. This is necessarily an approximation, also, since some configuration states mix strongly with one another. However, the way we have set up the calculation allows us to make a good guess. If we neglect the effect of off-diagonal configuration matrix elements we get a spectrum which can be separated into individual channels and the sum of which looks substantially like the configuration-mixed one. From this information, we conclude that the $J=0$ state is a pure $((d_{3/2})(p_{3/2})^{-1})$ state. The low-lying and high-lying $J=1$ states are primarily $((d_{5/2})(p_{3/2})^{-1})$ and $((d_{3/2})(p_{3/2})^{-1})$, respectively. The two $J=2$ states are primarily $((d_{5/2})(p_{3/2})^{-1})$ and $((d_{3/2})(p_{3/2})^{-1})$ for the lower and upper states, respectively. We shall see that the two bound states are primarily $((s_{1/2})(p_{3/2})^{-1})$. Although the s wave contains a continuum contribution, it is nonresonant and relatively flat. This is true for square-well wave functions regardless of whether the state is above or below threshold, in contrast to configuration states with $l>0$. Therefore, the s wave leads to sharp states below threshold but not above, except in special cases which will be discussed in the case of O^{16}.

TABLE III. Partial capture rate contributions to μ capture in C^{12}. The bound states and continuum contributions are listed separately.

J		M_V^2	M_A^2	M_P^2
0	Continuum		0.065	0.194
	Bound states		0.000	0.000
	Total		0.065	0.194
1	Continuum	0.509	0.180	
	Bound state	0.002	0.009	
	Total	0.511	0.189	
2	Continuum		0.256	0.307
	Bound state		0.005	0.006
	Total		0.261	0.313
	Total	0.511	0.515	0.507
	deForest results	0.567	0.562	0.550

The bound states have their configuration mixing parameters listed in Table II. The equivalent harmonic-oscillator theory results are listed for comparison. The results are clearly dominated by the s wave in both cases, but the signs of the other contributions are incompatible. We believe this is due to the peculiar nature of the s-wave bound states and their relationship to our model. The s wave, alone of the various contributions, does not have an angular momentum barrier. Thus the major part of its wave function lies close to $r=0$. The other l-wave contributions do not have this property; their bound-state wave functions vanish for $r=0$, rise fairly rapidly to a peak and descend again. The δ-function force which we used to solve the coupled bound-state problem has a different effect in the two cases when used to shift the energies of single-particle bound states. This energy shift arises from a discontinuity in the derivative of the bound wave function at the well radius. Because the bulk of the s wave lies close to the origin, it is difficult for this discontinuity to change the energy of the bound state. It is less difficult for $l\neq 0$. This is borne out in numerical calculations. The quantity $V_\beta'(E)$, introduced earlier, which we noted replaces $(E-E_\beta^0)$ in earlier bound-state calculations, as a function of energy is substantially larger than $(E-E_\beta^0)$ for the s-state case. It is slightly smaller than $(E-E_\beta^0)$ for the d-wave case. This leads to a depression of the energy of states which have a substantial s-wave contribution, as compared with other models. It can also have a strong effect on the configuration mixing coefficients as we see in Table II. The two bound-state cases which we investigated that did not have a substantial s-wave contribution have configuration mixing coefficients in reasonable agreement with the harmonic-oscillator shell model.

We now discuss the results of the μ-capture calculation. We noted before that there are four independent contributions to μ-capture partial-capture rates, two for $J^\pi=1^-$ and one each for $J^\pi=0^-$ and $J^\pi=2^-$. The broad high-lying $J^\pi=0^-$ state contributes only to M_A^2 and M_P^2 as do the two resonant and one bound $J^\pi=2^-$ states. Most of the $J=2$ strength, as we see in Fig. 2(d), lies in the giant quadrupole state at 20.0 MeV, in agreement with the results of deForest.[4] Further-

TABLE IV. Dipole and unretarded dipole capture rates and their ratios in C^{12}.

	(M_V^2)	(M_A^2)	(M_P^2)
Dipole	0.511	0.515	0.507
Unretarded dipole	0.727	0.745	0.732
Ratio $(M^2)_D/(M^2)_{UD}$	0.704	0.693	0.692
$\mid F_0(\nu_{res}^2) \mid^2$	0.698		

more, the $M_V^2(J=1)$ result seems, in Fig. 2(b), totally dominated by the giant dipole resonance at 22.8 MeV. Little sign of the 25.6-MeV state is visible. The $M_A^2(J=1)$ spectrum, however, has a strong contribution from this same 25.6-MeV state. The explanation for this lies in the two types of operators which cause transitions to $J=1$ states. One of these is the usual dipole operator Y_{1M} which produces transition primarily to states with large electric dipole moments (giant dipole states). The other is the magnetic operator $(Y_1\otimes\sigma)_{1M}$, which dominates spin-flip-type transitions. Both operators contribute to electron scattering as we see in Eq. (20). We can thus identify the 22.8-MeV state as the giant dipole resonance and the 25.6-MeV state as a "magnetic" state. We expect the momentum dependence of the two states to be quite different in electron scattering form factors, and we shall see later that this is indeed the case.

The results of integrating over the whole continuum spectrum to test the $SU(4)$ relationship $M_V^2=M_A^2=M_P^2$ are shown in Table III. The bound-state contributions are listed separately. We also list deForest's results for comparison.

We see that our over-all agreement is about 2%. The fact that the numbers are all smaller than the deForest calculation is likely due to the fact that this calculation omitted the high-lying $((p_{1/2})(s_{1/2})^{-1})$ state while deForest's did not. This state must necessarily make a positive contribution to the $J=0$ and $J=1$ transition rates.

Table IV lists the total strengths of the unretarded dipole contributions, the strengths of the retarded contributions, their ratio, and the ground-state elastic form factor for a momentum transfer corresponding to the energy of excitation of the giant dipole resonance. We see that the three equations

$$(M_{V,A,P^2})_D=(M_{V,A,P^2})_{UD}\mid F_0(\nu_{res}^2)\mid^2$$

hold to about 1%, as they did in deForest's results.

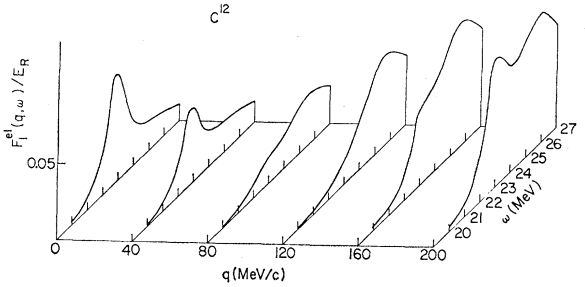

FIG. 4. C^{12} 1^- spectra for several momentum transfers. The "current" form of the transverse electric operator was used. E_R is $(\hbar c/r_0)$ $(=61.56$ MeV).

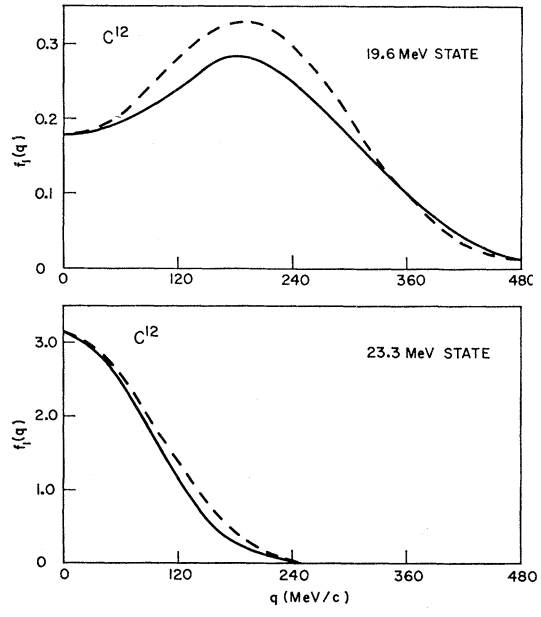

FIG. 3. C^{12} 1^- form factors versus momentum transfer. The "current" form factors $f_1(q)$ (dashed curve) and "charge" form factors $f_1'(q)$ (solid curve) normalized to the "current" form factors were calculated in the HOSM.

We now examine the electron scattering results. First we wish to demonstrate that, in the absence of magnetic effects, the two forms of the 1^- transverse electric operator give form factors which are roughly proportional. To test this we set $(\lambda_p-\lambda_n)=0$ and calculated the form factors of the 1^- states using the two different forms of the transition operator, $\hat{T}'_{JM}{}^{el}$ and $\hat{T}_{JM}{}^{el}$. The model used was the harmonic-oscillator shell model of Lewis and Walecka,[1] because this model allows a clean separation of individual states, which cannot be done in our continuum model. The form factors for $\hat{T}'_{1M}{}^{el}$ were normalized to those of $\hat{T}_{1M}{}^{el}$, and the results for two states were plotted in Fig. 3. We see that the agreement is quite good for these states. Unfortunately the form factor of the 1^- magnetic state in this model is negligible in the absence of the magnetic moment term, so no comparison could be made. The agreement of the other form factors is sufficiently good that we believe the form of our normalized form factors, regardless of which operator is used to calculate them. Similar results are obtained in the continuum model if the area under the giant resonance is calculated.

Figure 4 displays the 1^- form factor $F_1{}^{el}(q,\omega)$, which was calculated using the usual convection-current form of the transverse electric operator. The $q=0$ spectrum

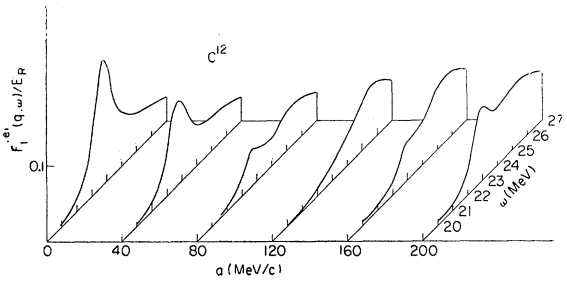

FIG. 5. C^{12} 1^- spectra for several momentum transfers. The "charge" form of the transverse electric operator was used. E_R is $(\hbar c/r_0)$ $(=61.56$ MeV).

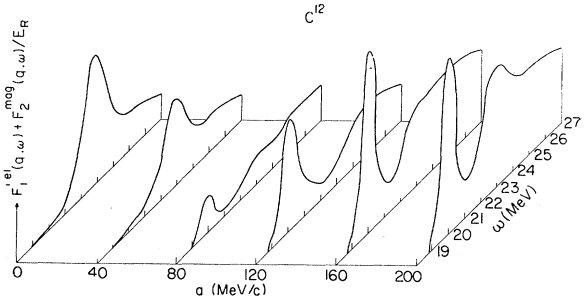

FIG. 7. Sum of C^{12} 1^- and 2^- spectra for several momentum transfers. The 1^- form factors were calculated using the "charge" form of the transverse electric operator. E_R is $(\hbar c/r_0)$ $(=61.56$ MeV).

is completely dominated by the giant resonance, while the magnetic state at 25.6 MeV is almost invisible. As the momentum transfer increases, the giant state decreases until at $q\approx120$ MeV/c it has entirely disappeared. As momentum transfer increases further, the state builds up its strength again until it reaches its initial value at $q\approx200$ MeV/c. The magnetic state immediately builds in strength, completely dominating the spectrum for $q>80$ MeV/c. We contrast this behavior with the results of Fig. 5, which displays the 1^- form factor $F'_1{}^{el}(q, \omega)$ calculated using the transverse electric operator $T'_{JM}{}^{el}$, which was discussed in detail earlier. The giant state has the same dependence on momentum transfer in the two cases but the magnetic state has a smaller influence. This is because the convection-current matrix element has been effectively doubled while the magnetic matrix element remained as before. Figure 6 shows the 2^- form factor $F_2{}^{mag}(q, \omega)$. This form factor vanishes for q near zero and rises rapidly with increasing q $(\sim q^4)$. The very prominent giant quadrupole state at 20.0 MeV dominates every spectrum. Because of its proximity to threshold, it is very narrow, while the other quadrupole state is much broader.

Figure 7 shows the sum of the contributions of $F'_1{}^{el}(q, \omega)$ and $F_2{}^{mag}(q, \omega)$. The resulting sum should be the prediction of $SU(4)$ invariance for the complete 1^- and 2^- spectrum.

Figure 8 shows the result of integrating the form factors $F_1{}^{el}(q, \omega)$ and $F_2{}^{mag}(q, \omega)$ over the giant resonance region. We define integrated form factors

$$f_J(q) = \int_{\omega_1}^{\omega_2} F_J(q, \omega)\, d\omega.$$

We have chosen $\omega_1=21.0$ MeV and $\omega_2=27.0$ MeV. Figure 9 shows the sum of the integrated form factors for $F'_1{}^{el}(q, \omega)$ $[f_1'(q)]$ and for $F_2{}^{mag}(q, \omega)$ $[f_2(q)]$. We have normalized this total form factor to the photoabsorption point at 23 MeV/c.

Although the experimental points have a considerable spread, it is clear that the integrated form factor

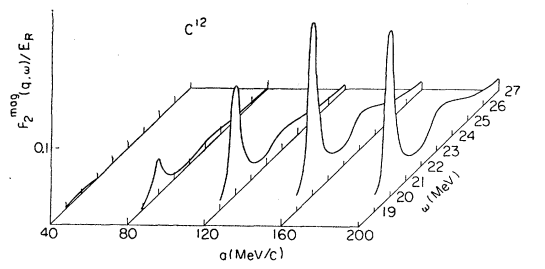

FIG. 6. C^{12} 2^- spectra for several momentum transfers. E_R is $(\hbar c/r_0)$ $(=61.56$ MeV).

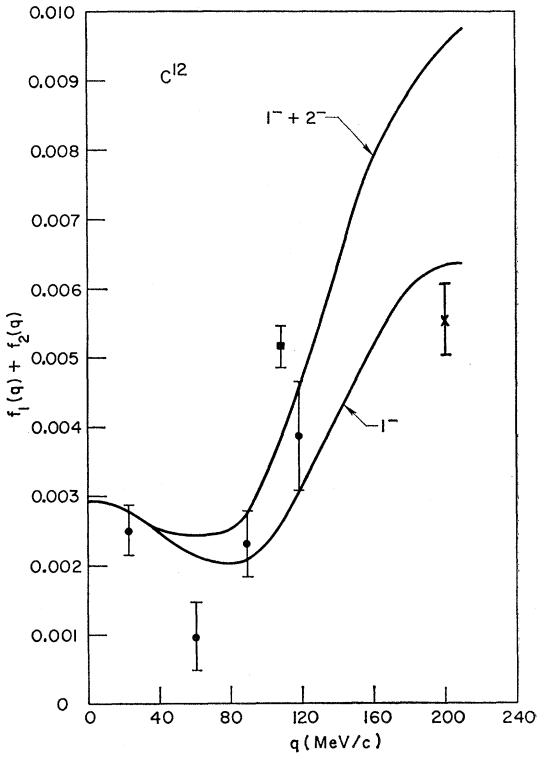

FIG. 8. C^{12} 1^- and 2^- integrated form factors for the giant resonance region. The lower curve is the 1^- "current" form factor; the upper curve includes the 2^- form factor as well. The data are from Refs. 1, 5, 41, and G. A. Proca and D. B. Isabelle, Nucl. Phys. **A109**, 177 (1968).

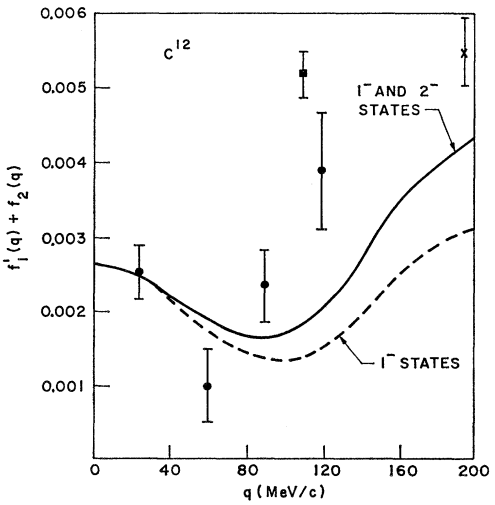

FIG. 9. C^{12} 1^- and 2^- integrated form factors for the giant resonance region normalized to the first data point. The lower curve is the 1^- "charge" form factor; the upper curve includes the 2^- form factor also. The data are from Refs. 1, 5, and 41.

seen experimentally has a dip for $q\approx 80$ MeV/c. This dip is clearly visible in both Figs. 8 and 9. Although Fig. 8 seems to give a good fit to both low- and high-momentum transfers, (with the exception of the point at 60 MeV/c), Fig. 9 is probably closer to reality. Higher multipoles contributing to the integrated form factor will become important for $q>100$ MeV/c and will build up the curve. Also, if the point at 60 MeV/c is to be believed, the form factor $f_1(q)$ does not have enough of a dip. Between the two cases, however, the experimental points are fairly well bracketed. The reason for the different behaviors at high-momentum transfers can be attributed to the different roles played by the magnetic 1^- state at 25.6 MeV. As we saw in Fig. 4, this state rises rapidly with increasing momentum transfer and dominates the spectrum. In Fig. 5, however, this state was not so dominant, owing to the reduction that was made of the current operator. This reduction approximately doubled the strength of the giant resonance at $q=0$, while leaving the magnetic state's strength alone. Because of this, the high-momentum transfer behavior in the two cases is different. It is somewhat difficult to see all this in the continuum model we have used, but it is readily apparent in the model of Lewis and Walecka[1] which allows form factors for individual states to be calculated separately.

The integrated form factor for the 2^- state at 20.0 MeV, $f_2(q)$, was calculated using $\omega_1=19.0$ MeV and $\omega_2=21.0$ MeV in the previous equation. This form factor is plotted in Fig. 10. The form factor reduced by the ratio of the experimental photoabsorption cross section to the theoretical one (from $\hat{T}'_{1M}{}^{el}$) is also plotted. This is the $SU(4)$ prediction. The unreduced form factor is somewhat higher than experiment, although not the factor of 2 higher predicted by deForest.[4] The reduced form factor is probably much too low.

The backscattering data of deForest *et al.*[41] at $q\approx 110$ MeV/c can be compared to the results of our calculation. We note that in Fig. 7 there is no giant resonance at this momentum transfer, although the magnetic state at 25.6 MeV is large. The bump at 25 MeV would appear to correspond to this state. The giant quadrupole state at 20.0 MeV would appear to correspond to the state seen at 19.2 MeV in the experimental data. There are two states at approximately the correct energies to correspond to the two bound states (1^- and 2^-). The 23.7-MeV state may correspond to the uppermost 2^- state that we have calculated, although it is difficult to see because it is fairly small and rather wide.

Discussion of O^{16}

The procedure for O^{16} is the same as for C^{12}. Single-particle configuration energies are taken from neighboring nuclei O^{15} and O^{17}. Oxygen consists of filled $1s_{1/2}$, $1p_{3/2}$, and $1p_{1/2}$ shells. Ignoring the low-lying $1s_{1/2}$, we are left with two possible hole states. As in the case of C^{12}, there are three particle states which can be used to form negative-parity particle-hole states, $s_{1/2}$, $d_{3/2}$, and $d_{5/2}$. There six possible configurations of which two contribute to $J^\pi=0^-$, and 5 each to $J^\pi=1^-$, 2^-. These configurations and their configuration energies[2] are

$$E^0((1d_{5/2})(p_{1/2})^{-1})=11.52 \text{ MeV},$$
$$E^0((2s_{1/2})(p_{1/2})^{-1})=12.39 \text{ MeV},$$
$$E^0((1d_{3/2})(p_{1/2})^{-1})=16.60 \text{ MeV},$$
$$E^0((1d_{5/2})(p_{3/2})^{-1})=17.68 \text{ MeV},$$
$$E^0((2s_{1/2})(p_{3/2})^{-1})=18.55 \text{ MeV},$$
$$E^0((1d_{3/2})(p_{3/2})^{-1})=22.76 \text{ MeV}.$$

The single-particle energies can now be used to determine the well radius r_0 and the configuration potential depths. Using[42]

$$R_{\text{rms}}=2.65\pm 0.04 \text{ fm},$$

we get

$$r_0'=1.40 \text{ fm}$$

as before.

Using the photoabsorption cross section we can determine the over-all potential strength V_0 by forcing the O^{16} giant resonance state to have its peak at 22.4 MeV. We get

$$V_0=-24.4 \text{ MeV}.$$

An examination of the electron scattering and μ-capture spectra allows us to determine the widths and energies of the resonance states (Table V). Because the O^{16} spectra for μ capture and electron scattering are quite similar to the C^{12} results, the detailed drawings

[41] T. deForest, Jr., J. D. Walecka, H. VanPraet, and W. C. Barber, Phys. Letters **16**, 311 (1965).
[42] H. Crannell, Phys. Rev. **148**, 1107 (1966).

have been omitted. The results, however, are discussed. The $J=0$ spectrum consists of a single large state at 25.4 MeV with a width of about 1.5 MeV. This state is primarily a $((d_{3/2})(p_{3/2})^{-1})$ configuration. The $J=2$ spectrum consists of 4 resonances. The 23.4-MeV state has a width of about 0.4 MeV and is primarily a $((d_{3/2})(p_{3/2})^{-1})$ configuration. The giant quadrupole state is very narrow, $\sim$0.2 MeV and is primarily a $((d_{5/2})(p_{3/2})^{-1})$ configuration. Although this state lies below the $p_{3/2}$ hole separation energy, the state acquires a width (albeit small) through configuration mixing. The other two states are caused by a similar phenomenon noted by Weiss in his work on photoexcitation in O^{16}.[24] The $((d_{3/2})(p_{1/2})^{-1})$ configuration state can lead to two states through virtual excitation into the nonresonant s-wave channel $((s_{1/2})(p_{3/2})^{-1})$ and back down again. In the process a new resonance is formed. If configuration mixing between the $p_{1/2}$ hole states and the $p_{3/2}$ hole states is turned off, the two resonances become a single one. Both these resonances are very narrow, $\sim$0.15 MeV. The structure of the $J=1$ spectrum is similar. The 25.2-MeV state has a width of about 2 MeV and is primarily a $((d_{3/2})(p_{3/2})^{-1})$ configuration. The giant dipole resonance with a width of about 1 MeV is primarily $((d_{5/2})(p_{3/2})^{-1})$. The same state-splitting mechanism holds for the $J=1$ spectrum also. The two states have widths of about 0.15 MeV.

The bound-state mixing parameters are listed in Table VI with the harmonic-oscillator model results of Lewis and deForest listed for comparison. We see that the best agreement is the $J=2$ state. This state is primarily $((d_{5/2})(p_{1/2})^{-1})$, rather than $((s_{1/2})(p_{1/2})^{-1})$, as the others are. In fact, the only mixing parameter which

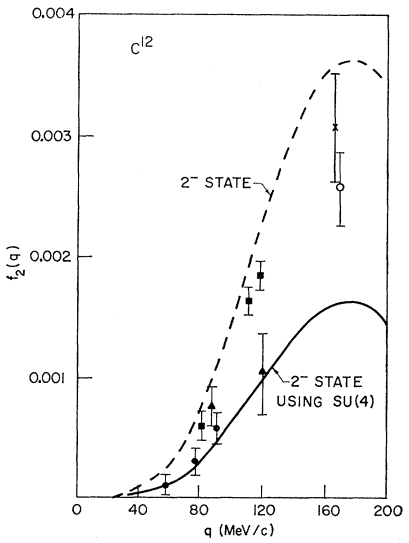

FIG. 10. C^{12} integrated form factor for the 2^- 20.0-MeV state. The solid curve is reduced by the ratio of theoretical to experimental integrated photoabsorption spectrum. The data are from Refs. 5, 41, and G. A. Proca and D. B. Isabelle, Nucl. Phys. A109, 177 (1968); and G. A. Beer, T. E. Drake, R. M. Hutcheon, and H. C. Caplan, Nuovo Cimento 53B, 319 (1968).

TABLE V. Energies of bound states and resonances in O^{16}. Energy in MeV.

$J=0$	$J=1$	$J=2$
13.31	13.23	12.52
25.4	17.2	17.7
	19.1	18.2
	22.4	20.6
	25.2	23.4

is not substantially in agreement is the $((s_{1/2})(p_{3/2})^{-1})$ term. For previously mentioned reasons, the $s_{1/2}$ particle states lead to disagreements between the results of the two models.

The O^{16} μ-capture results indicate that the $J^\pi=1^-$ 19.1-MeV state and the 25.2-MeV state are primarily magnetic. The strength of these states in the $M_A{}^2(J=1)$ spectrum indicates that they are easily excited by the magnetic operator $(Y_1\otimes\sigma)_1$. The 20.6-MeV giant quadrupole state dominates the $J=2$ μ-capture spectrum, as one would expect. The lone $J^\pi=0^-$ resonance at 25.4 MeV contributes virtually all the $J=0$ strength (in the continuum) in spite of the mixture of the nonresonant $((s_{1/2})(p_{1/2})^{-1})$ state. Most of the strength of the latter configuration is in the low-lying $J=0$ bound state. The giant resonance dominates the $M_V{}^2(J=1)$ spectrum. We present the results of integrating over the whole spectrum of $M_V{}^2$, $M_A{}^2$, and $M_P{}^2$ in Table VII. Bound and continuum contributions are separately listed, and deForest's harmonic-oscillator results are included for comparison.

The agreement on $M_P{}^2=M_A{}^2=M_V{}^2$ is about 9%, while the agreement on the relationship

$$(M_{V,A,P}{}^2)_D=(M_{V,A,P}{}^2)_{UD}\mid F_0(\nu_{\rm res}{}^2)\mid^2$$

is within 3% (Table VIII). In agreement with deForest's results, $M_V{}^2$ is lower than $M_A{}^2$ and $M_P{}^2$. Unlike the C^{12} results, however, the ratios $(M^2)_D/(M^2)_{UD}$ are all larger than the elastic form factor.

The role of the charge and current operator in $\hat{T}_1{}^{\rm el}$ was also investigated in O^{16} in the harmonic-oscillator shell model. Setting $(\lambda_p-\lambda_n)$, the isovector nucleon magnetic moment, equal to zero, several different form factors were calculated using the two forms of $\hat{T}_1{}^{\rm el}$. As in the case of C^{12}, the resulting form factors are nearly the same.

The upper portion of the energy spectrum of the 1^- form factor $F_1{}^{\rm el}(q,\omega)$ displays a not very surprising resemblance to the C^{12} spectrum. The giant dipole state dominates at small momentum transfers. Although the magnetic state at 25.2 MeV can be easily distinguished, it is relatively small. The two states lying below the $p_{3/2}$ threshold are also quite small. As momentum transfer increases the magnetic state becomes quite large, dominating the spectrum for $q>60$ MeV/c. The giant dipole state decreases until it vanishes for $q\approx120$ MeV/c

TABLE VI. Configuration mixing parameters for the bound states in the HOSM and continuum model for O^{16}.

		$((s_{1/2})(p_{1/2})^{-1})$	$((d_{5/2})(p_{1/2})^{-1})$	$((d_{3/2})(p_{1/2})^{-1})$	$((s_{1/2})(p_{3/2})^{-1})$	$((d_{5/2})(p_{3/2})^{-1})$	$((d_{3/2})(p_{3/2})^{-1})$
	13.31 MeV						
$J=0$	Continuum	0.990					−0.140
	Harmonic oscillator	0.998					0.070
	13.23 MeV						
$J=1$	Continuum	0.968		0.014	−0.009	0.245	0.051
	Harmonic oscillator	0.991		−0.011	−0.063	−0.113	−0.029
	12.52 MeV						
$J=2$	Continuum		0.977	0.019	−0.142	0.150	0.048
	Harmonic oscillator		0.974	−0.025	0.069	0.201	0.076

and then increases again. The higher of the two lowest resonances displays a large growth as q increases, confirming the original indication in μ capture that it had a magnetic behavior (magnetic 1^- states grow like q^4, just as 2^- states do). The other state grows also but is smaller than its companion.

The form factor $F'_1{}^{el}(q, \omega)$ also has many characteristics of the equivalent C^{12} figure. The giant resonance vanishes and rises as before, but the 25.2-MeV magnetic state shows less activity. We shall see that this is strongly reflected in the integrated form factors. The 19.1-MeV state shows its usual magnetic character, although the companion state does not move appreciably.

All of the resonances which contribute to the 2^- form factor $F_2{}^{mag}(q, \omega)$ show their magnetic behavior clearly. The most interesting feature is the fact that the two lowest-lying states are close enough to coalesce, giving something of the appearance of a single broad state.

TABLE VII. Partial capture rate contributions to μ capture in O^{16}. The bound-state and continuum contributions are listed separately.

J		$M_V{}^2$	$M_A{}^2$	$M_P{}^2$
0	Continuum		0.084	0.253
	Bound state		0.006	0.016
	Total		0.090	0.269
1	Continuum	0.900	0.293	
	Bound state	0.000	0.005	
	Total	0.900	0.298	
2	Continuum		0.409	0.490
	Bound state		0.187	0.224
	Total		0.596	0.715
	Total	0.900	0.983	0.984
	deForest results	0.857	0.938	0.938

Figure 11 displays the sum $F_2{}^{mag}(q, \omega)$ and $F'_1{}^{el}(q, \omega)$, giving the best $SU(4)$ prediction for a scattering form factor.

Figure 12 shows the integrated form factor $f_1(q)+f_2(q)$. The range of integration is the same as in C^{12}. Although the over-all normalization is a little low (15–20%), the shape of the curve agrees with the experiments if one believes the first (photoabsorption) point. If this point is low, then oxygen will also show the pronounced dip seen in C^{12}. This would be even more pronounced in the form factor $f_1'(q)+f_2(q)$ normalized to the *second* experimental point. This form factor looks much like carbon, being too small for large q. Higher multipoles would presumably build the curve up at higher momentum transfers. Because the magnetic state does not build rapidly in the case represented by $f_1'(q)$, the effect of the rapid decrease in strength of the giant resonance is emphasized, causing a dip. The magnetic state in the other case rises rapidly enough to offset this effect, resulting in a flatter form factor.

The fact that both form factors $f_1(q)$ are somewhat smaller than the ones calculated in the harmonic-oscillator shell model is probably due to the fact that the broad magnetic state has strength outside the range of integration. In a pure bound-state model, all the strength is concentrated at the bound-state's energy eigenvalue.

The 20.6-MeV 2^- form factor f_2 was also calculated,

TABLE VIII. Dipole and unretarded dipole capture rates and their ratios in O^{16}.

	$(M_V{}^2)$	$(M_A{}^2)$	$(M_P{}^2)$
Dipole	0.900	0.984	0.983
Unretarded dipole	1.37	1.50	1.50
Ratio $(M^2)_D/(M^2)_{UD}$	0.657	0.654	0.655
$F_0{}^2(\nu_{res}{}^2)$	0.639		

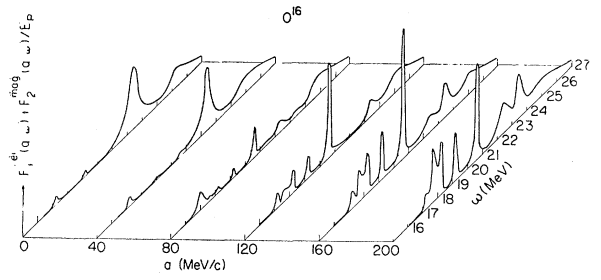

FIG. 11. Sum of the O^{16} 1^- and 2^- spectra for several momentum transfers. The 1^- form factors were calculated using the "charge" form of the transverse electric operator. E_R is $(\hbar c/r_0)$ $(=55.9$ MeV).

the range of integration being 20–21 MeV. This form factor behaves very nearly the same as the corresponding 20.0-MeV one in C^{12}. We see in Fig. 13 that it lies above the experimental results, but not by the factor of 2 predicted by deForest.[4] When normalized to the integrated photoabsorption cross section, the resulting curve is rather low. A similar plot for the 2^- bound state at 12.52 MeV is shown in Fig. 14. This form factor is a little higher than the prediction of deForest, but the normalized form factor seems to fit the experimental data nicely. The bound 1^- state which lies nearby has a negligible transverse form factor compared to the 2^- state, so that its inclusion in the overall transverse form factor for this region has little effect. Both 2^- states are observed in inelastic proton scattering and they adequately account for the cross-sections seen.[43,44]

Figure 15 shows the form factor $f_1(q)$ for the 1^- 17.2-MeV state, using $\omega_1=16.0$ MeV and $\omega_2=18.0$ MeV. This result is in quite good agreement with the experimental data. The results of Lewis[2] for this state

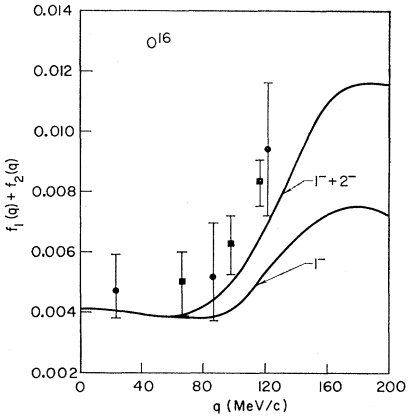

FIG. 12. O^{16} 1^- and 2^- integrated form factors for the giant resonance region. The lower curve is the 1^- "current" form factor; the upper curve includes the 2^- contribution as well. The data are from Ref. 5, 7, and E. G. Fuller and E. Hayward, in *Nuclear Reactions*, edited by P. M. Endt and P. B. Smith (North-Holland Publishing Co., Amsterdam, 1962), Vol. II.

[43] T. Erickson, Nucl. Phys. **54**, 321 (1964).
[44] H. K. Lee and H. McManus, Phys. Rev. **161**, 1087 (1967).

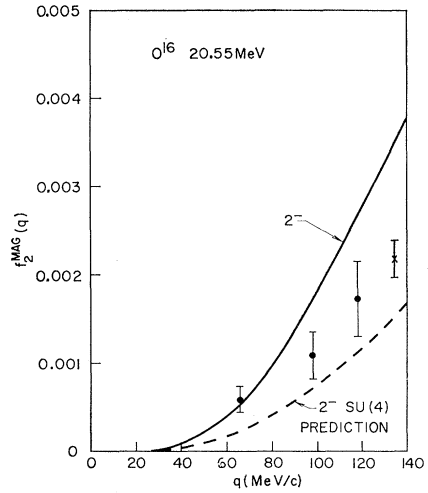

FIG. 13. O^{16} integrated form factor for the 2^- 20.55-MeV state. The dashed curve is reduced by the ratio of the theoretical result to the experimental result for the integrated photoabsorption spectrum. The data are from Ref. 6 and T. E. Drake, E. L. Tumusiak, and H. S. Caplan, Nucl. Phys. **A118**, 138 (1968).

give a form factor which is approximately twice as large as experiment.

Figure 11 can be compared with the backscattering results of VanPraet[7] for 69-MeV incident electrons. The approximate momentum transfer is 120 MeV/c $(q=2E_i-\omega)$. As in the carbon case, the calculation shows no giant resonance at this momentum transfer. There are a number of other prominent states, however. The two bound-states at 12.5 and 13.2 MeV are close to two peaks in the cross section at 12.2 and 13.0 MeV. There are three states rather close together between 17.2 and 18.2 MeV, while the experimental data shows a bump at 17.1 MeV and possibly one between 18.0 and 18.7 MeV. There is a predicted 1^- state at 19.1 and a prominent bump at 19.2 in the experimental

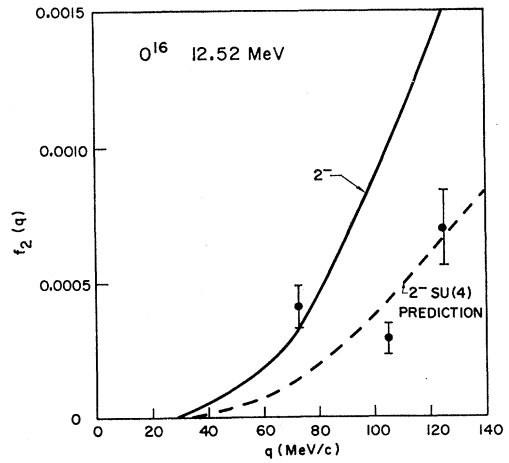

FIG. 14. O^{16} form factor for the 2^- 12.52-MeV state. The dashed curve is reduced by the ratio of the theoretical result to the experimental result for the integrated photoabsorption spectrum. The data are from Ref. 6.

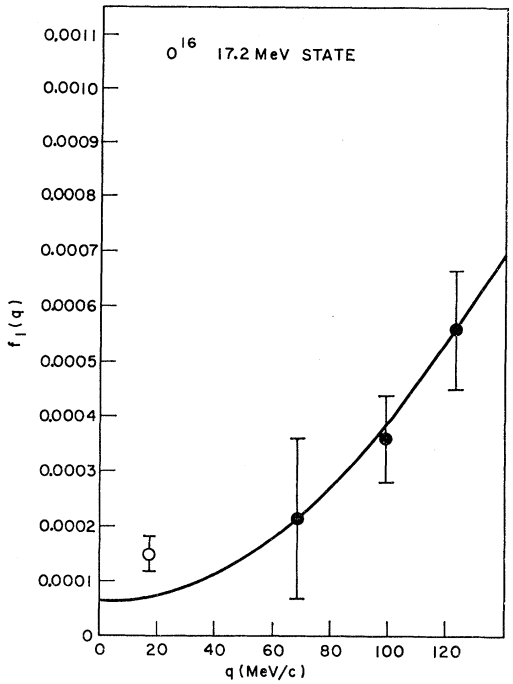

FIG. 15. O^{16} integrated form factor for the 17.2-MeV 1^- state. The data are from Refs. 6 and E. G. Fuller and E. Hayward, in *Nuclear Reactions*, edited by P. M. Endt and P. B. Smith (North-Holland Publishing Co., Amsterdam, 1962), Vol. II.

cross section. The giant quadrupole state at 20.6 MeV seems to match the 20.4-MeV experimental peak. The other predictions are the 2^- state at 23.4 MeV and the 25.2-MeV 1^- state. The two most prominent peaks seen in the experimental data in this energy range are at 23.8 and 26.0 MeV and presumably correspond to the above predictions. Although the predicted widths are much narrower in most cases than the experiments indicate, the experimental resolution is probably little better than 1 MeV.[45] This would make narrow states appear much broader.

Another point must be made about the behavior of the giant dipole resonance and the high-lying 1^- magnetic state. We saw above that the detailed behavior of the two states is not in good agreement with experiment, although the integrated form factor (21–27 MeV) is in rough agreement. We can give one possible explanation of this by simplifying the model to the barest essentials. Let us consider configuration mixing in the HOSM, where we will only include the $((1d_{5/2})(1p_{3/2})^{-1})$ and the $((1d_{3/2})(1p_{3/2})^{-1})$ configurations. These are the largest contributions to the above-mentioned states. We denote the first of the above particle-hole configuration states by $(\mathrm{ph})_1$ and the second by $(\mathrm{ph})_2$. Our two configuration-mixed states are therefore

$$\psi_1=\alpha(\mathrm{ph})_1+\beta(\mathrm{ph})_2,$$

$$\psi_2=-\beta(\mathrm{ph})_1+\alpha(\mathrm{ph})_2,$$

[45] W. C. Barber (private communication).

where ψ_1 and ψ_2 are the giant dipole resonance and the 1^- magnetic state, respectively. The transition probabilities can therefore be written

$$T^{(1)}\equiv\langle\psi_1\,||\,\hat{T}\,||\,0\rangle=\alpha t_1+\beta t_2,$$

$$T^{(2)}\equiv\langle\psi_2\,||\,\hat{T}\,||\,0\rangle=-\beta t_1+\alpha t_2,$$

where

$$t_1=\langle(\mathrm{ph})_1\,||\,\hat{T}\,||\,0\rangle,$$

$$t_2=\langle(\mathrm{ph})_2\,||\,\hat{T}\,||\,0\rangle.$$

The detailed behavior of $|\,T^{(1)}\,|^2$ and $|\,T^{(2)}\,|^2$ obviously are sensitive to the sign and magnitude of β. Yet if we form

$$\sum_i|\,T^{(i)}\,|^2,$$

we get

$$\sum_i|\,T^{(i)}\,|^2=(\alpha^2+\beta^2)\sum_i|\,t_i\,|^2=\sum_i|\,t_i\,|^2,$$

since $\alpha^2+\beta^2=1$ is the normalization condition of our states. This interesting result for the integrated form factor is now independent of α and β and therefore independent of the particle-hole potential. In essence we have a sum rule. We therefore see that our integrated form factors are much less sensitive to details of the model (such as the potential) than is the behavior of each individual state.

SUMMARY

In summary, we see that a "realistic model" of the giant resonance region has been examined. This model allowed construction of particle-hole states in the continuum and was capable of analytic solution. Using the model, spectral surfaces in q (momentum transfer) and ω (energy loss) were constructed for electron scattering as well as the neutrino spectrum in μ capture.

In μ capture the $SU(4)$ relationship

$$M_V^2=M_P^2=M_A^2$$

was tested in C^{12} and O^{16}. While this relationship does not hold for individual levels or resonances (we do not expect it to), the agreement is good when all levels have been summed over. The relationship held to within 3% in C^{12} and within 9% in O^{16}, even though the over-all size of the individual matrix elements was off by a factor of 2. This agreement justified the work of Foldy and Walecka.[46] In addition, we tested the relationship

$$(M_V^2)_D=(M_V^2)_{UD}\,|\,F_0(\nu_{\mathrm{res}}^2)\,|^2$$

in our model and found that the discrepancy was only 1% in C^{12} and 3% in O^{16}. It should be noted that our model has a continuous spectrum from the lowest threshold upwards, so that it was necessary to include the rather long "tails" of some of the resonances in the

[46] This analysis was successful because of the weak spin dependence of the particle-particle potential. For a different point of view using another model see Ref. 12.

calculation. This contrasts with the usual bound-state models.

In electron scattering we calculated the transverse form factors for 1^- and 2^- states because these form factors show the importance of magnetic effects. These results were compared with experiment, and the predicted levels are generally seen. The integrated form factors that can be derived from the energy spectra show reasonably good agreement with experiment. We have also seen that normalizing certain form factors by the ratio of experimental to theoretically predicted integrated photoabsorption cross sections improves the results, again pointing out the importance of $SU(4)$ to the nuclear physics of the giant resonances. The widths we predict for our states are in qualitative agreement with experiment. This model also justifies previous identification of narrow giant quadrupole states predicted by deForest. We have also investigated why the high-lying magnetic 1^- state does not become huge at large momentum transfers, although shell-model calculations, including this one, predict a vanishing of the giant dipole resonance for momentum transfers $q \approx 120$ MeV/c due to interference between the electric and magnetic parts of the 1^- transverse operator. This is not seen experimentally.

ACKNOWLEDGMENT

The author would like to thank Professor J. D. Walecka for suggesting this problem and for his helpful criticism and enlightening discussion.

PHYSICAL REVIEW C VOLUME 1, NUMBER 1 JANUARY 1970

Structure of the Nucleon-Nucleus Scattering Matrix in the Random-Phase Approximation*

J. N. Ginocchio, T. H. Schucan,† and H. A. Weidenmüller‡
Physics Department, Yale University, New Haven, Connecticut 06520

(Received 20 May 1969)

The scattering matrix is derived for the scattering of nucleons by nuclei lacking one nucleon from being doubly magic. It is assumed that an average field has been determined through a Hartree-Fock procedure (HF). The residual interaction is treated in the random-phase approximation (RPA). In contrast to previous treatments, it is not assumed that this interaction is separable. The RPA ground state of the compound system is given by a correlated wave function $|\Psi_0\rangle$. It is assumed that states of the target and residual nucleus can be described as one-hole states in this correlated ground state $|\Psi_0\rangle$. It is found that the RPA equations allow for a proper definition of asymptotic states only if the full Hamiltonian (including the c.m. energy) is used in the HF procedure. A general, yet explicit, expression for the S matrix is obtained by applying to the channel-channel part of the residual interaction a method first proposed by Weinberg. The correlations contained in $|\Psi_0\rangle$ give rise to poles of the scattering matrix for real negative energies *below* the energy of the lowest bound state, i.e., the ground state $|\Psi_0\rangle$. In the energy region of physical interest, these poles have two effects on the scattering matrix. First, a constant background term is introduced. Second, the partial widths $\Gamma_{\lambda c}$ for decay of a compound state (λ) into an open channel (c) are complex. The sum of the partial widths, $\Sigma_{\lambda c}\Gamma_{\lambda c}$, is compared with the sum of the total widths, $\Sigma_\lambda \Gamma_\lambda$. It is found that the two sums differ by terms of second order in the admixture of correlations in the ground state. The influence of symmetry properties of the Hamiltonian on the RPA solutions is discussed. It is shown that the scattering matrix derived is that in the c.m. frame, and it is completely independent of the total momentum of the nucleus.

I. INTRODUCTION

THE random-phase approximation (RPA) is a useful tool for the understanding of collective properties of nuclear levels.[1] It serves primarily as a useful model in which the occurrence of collective modes of motion can be theoretically understood on a microscopic basis. Compared with the ordinary shell-model [or Tamm-Dancoff (TD)] treatment, the RPA offers an improved understanding of the relationship between symmetry properties of the Hamiltonian and the occurrence of collective modes.[2] The RPA also yields a semiquantitative account of the positions and electromagnetic properties of vibrational states.[3]

Since the RPA has turned out to be such a useful

* Work supported in part by the U.S. Atomic Energy Commission, under Contract No. AT(30-1)-3223 and AT(30-1)-2726.

† Present address: Institut für Theoretische Physik der Universität Heidelberg, Heidelberg, West Germany.

‡ On leave of absence from Heidelberg University and from the Max Planck Institut für Kernphysik, Heidelberg, Germany.

[1] M. Baranger, Phys. Rev. **120**, 957 (1960); R. Arvieu and M. Veneroni, Compt. Rend. **250**, 922 (1960); T. Marumori, Progr. Theoret. Phys. (Kyoto) **24**, 331 (1960); S. T. Beliaev and V. G. Zelevinsky, Nucl. Phys. **39**, 582 (1962).

[2] D. J. Thouless, Nucl. Phys. **22**, 78 (1961); D. J. Thouless and J. G. Valatin, *ibid.* **31**, 211 (1962).

[3] G. E. Brown, L. Castillejo, and J. A. Evans, Nucl. Phys. **22**, 1 (1961); G. E. Brown, J. A. Evans, and D. J. Thouless, *ibid.* **45**, 164 (1963); A. Goswami and M. K. Pal, *ibid.* **35**, 544 (1962); V. Gillet and N. Vinh Mau, *ibid.* **54**, 321 (1964); V. Gillet, A. M. Green, and E. A. Sanderson, *ibid.* **88**, 321 (1966); V. Gillet and E. A. Sanderson, *ibid.* **A91**, 292 (1967).